https://doi.org/10.5194/acp-2020-601
Preprint. Discussion started: 8 July 2020

Atmospheric Chemistry and Physics Discussions

First validation of GOME-2/MetOp Absorbing Aerosol Height using EARLINET lidar observations

Konstantinos Michailidis[1*], Maria-Elissavet Koukouli[1], Nikolaos Siomos[1], Dimitrios Balis[1], Olaf Tuinder[2], L. Gijsbert Tilstra[2], Lucia Mona[3], Gelsomina Pappalardo[3] and Daniele Bortoli[4,5]

[1]Laboratory of Atmospheric Physics, Physics Department, Aristotle University of Thessaloniki, Greece
[2]Royal Netherlands Meteorological Institute (KNMI), De Bilt, the Netherlands
[3]Consiglio Nazionale delle Ricerche – Istituto di Metodologie per l'Analisi Ambientale (CNR-IMAA), C. da S. Loja, TitoScalo (PZ), Italy
[4]Institute of Earth Sciences (ICT), Évora, Portugal
[5]Physics Department, University of Évora, Portugal

Correspondence to: Konstantinos Michailidis (komichai@physics.auth.gr)

Abstract. The aim of this study is to investigate the potential of the GOME-2 instruments on board the MetOpA, MetOpB and MetOpC platforms, to deliver accurate geometrical features of lofted aerosol layers. For this purpose, we use archived ground-based lidar data from lidar stations available from European Aerosol Research Lidar Network (EARLINET) database. The data are post-processed with the wavelet covariance transform (WCT) method in order to extract geometrical features such as the Planetary Boundary Layer, PBL, height and the cloud boundaries. To obtain a significant number of collocated and coincident GOME-2 – EARLINET cases for the period between January 2007 and September 2019, thirteen lidar stations, distributed over different European latitudes, contributed to this validation. For the 172 carefully screened collocations, the mean bias was found to be -0.18±1.68km, with a near Gaussian distribution. On a station-basis, and with a couple of exceptions where very few collocations were found, their mean biases fall in the ±1 km range with an associated standard deviation between 0.5 and 1.5 km. Considering the differences, mainly due to the temporal collocation and the difference between the satellite pixel size and the point view of the ground-based observations, these results are quite promising and demonstrate that stable and extended aerosol layers as captured by the satellite sensors, are verified by the ground-based data. We further present an in-depth analysis of a strong and long-lasting Saharan dust intrusion over the Iberian Peninsula. We show that, for this well-developed and spatially well-spread aerosol layer, most GOME-2 retrievals fall within 1km of the exactly temporally collocated lidar observation for the entire range of 0 to 150km radii. This finding further testifies to the capabilities of the MetOp-born instruments to sense the atmospheric aerosol layer height.

1. Introduction

Aerosols are important constituents of the atmosphere, influencing both the air quality and the Earth's climate. They scatter and absorb solar and terrestrial radiation (direct effect) and alter the physical, optical and lifetime properties of clouds and thus the precipitation formation (indirect effect), as they act as cloud condensation nuclei. However, the overall uncertainties in the radiative forcing effect of aerosols (anthropogenic and natural) remain very high still (IPCC, 2013). These uncertainties can only be reduced by better quantifying the vertical and horizontal distribution of aerosols over the globe. Knowledge of geometrical features of aerosol layers is essential for understanding the impact of aerosols on the climate system. The aerosol height quantification of smoke, dust, biomass burning aerosols as well as volcanic ash, is a

https://doi.org/10.5194/acp-2020-601
Preprint. Discussion started: 8 July 2020

critical determinant of global aerosol transport and dispersion. Moreover, the vertical distribution of aerosols varies depending on the weather conditions and their dynamic processes. In the framework of aviation safety, it is important to have accurate knowledge about the height of aerosol layers in the atmosphere since dust and ash particles can be transported over large distances away from their source and so global monitoring is essential (e.g., Balis et al., 2016). There are several differences in the sensing principles between active and passive remote sensing of aerosols, specifically in terms of vertical resolution. Lidar (Light detection and ranging) remote sensing techniques can provide accurate vertical profiles of the aerosol backscatter and extinction coefficients, which are representative of the aerosol load, with vertical resolution of a few meters. Active lidar sensors such as those belonging to the European Aerosol Research Lidar Network (EARLINET; Pappalardo et al, 2014) provide vertical information for the aerosol load over Europe, but have limited spatial coverage due to their individual locations. On the other hand, passive space borne remote sensing instrumentation has the ability to measure a specific point on Earth once a day for polar orbiting satellite missions and several times in the day for geostationary missions. Polar satellites such as the Meteorological Operational satellite programme (MetOp) series offer the advantage of global and daily coverage and instruments such as Global Ozone Monitoring Experiment–2 (GOME-2) have already been used for aerosol detection (Hassinen et al., 2016). Therefore, combined studies based on ground based lidars together with atmospheric satellites will allow full exploitation of this data for a detailed description of the temporal and spatial distribution and evolution on a global scale. In this study, a quantitative assessment of the Level 2 absorbing aerosol height product derived by the GOME-2 aboard the MetOp platforms (Munro et al. 2016; Hassinen et al., 2016), using EARLINET lidar data as reference. Furthermore a case study with several MetOp overpasses close to the EARLINET station of Évora, Portugal, (38.56°N, -7.91°E, 293m a.s.l) on 20-23 February 2017, is analyzed to demonstrate the performance of the GOME-2 AAH retrieval for a strong Saharan dust event.

This paper is organized as follows. In Sect. 2, the GOME-2/MetOp satellite-borne instrument and the European Aerosol Research Lidar Network (EARLINET) are described. The data and methodology are briefly described in Sect 3. Sect. 4 presents the network-based intercomparison results between GOME-2 and EARLINET and a selected dust case is shown so as to illustrate the evaluation methodology. Finally, Sect. 5 contains the summary and the conclusions of this article.

2. Satellite and ground-based instrumentation

2.1 Description of the GOME-2 instrument

The Global Ozone Monitoring Instrument (GOME-2) GOME-2 instrument, on board the MetOp-A, B and C platforms, is a UV–VIS–NIR (visible–near IR) nadir viewing scanning spectrometer, with an across-track scan time of 6 s and a nominal swath width of 1920 km, which provides global coverage of the sunlit part of the atmosphere within a period of approximately 1.5 days (Hassinen et al., 2016; Munro et al., 2016). The MetOp satellite series is the core element of the European Organization for the Exploitation of Meteorological Satellites (EUMETSAT) Polar System (EPS), developed in partnership with the European Space Agency, ESA. The primary GOME-2 instrument characteristics are listed in Table 1. The three Global Ozone Monitoring Experiment-2 instruments provide unique and long data sets for atmospheric research and applications. The complete mission time is expected to cover 2007-2024 period. The AC SAF (Satellite Application

https://doi.org/10.5194/acp-2020-601
Preprint. Discussion started: 8 July 2020

Facility on Atmospheric composition) is responsible for the development and distribution of the GOME-2 Level 2 products accessed through the AC SAF web portal, https://acsaf.org/product_list.html.

2.2 The EARLINET network

The EARLINET network was founded in 2000 as a research project for establishing a quantitative, comprehensive, and statistically significant database for the horizontal, vertical, and temporal distribution of aerosols on a continental scale (Bösenberg et al., 2003; Pappalardo et al., 2014). Since then EARLINET has continued to provide the most extensive collection of ground-based data for the aerosol vertical distribution over Europe. EARLINET is one of the components of ACTRIS, the European Aerosol Clouds and Trace gases Research Infrastructure, now in its implementation phase. Within ACTRIS, many developments have been realized in EARLINET improving the quality assurance of the lidar systems and the quality control procedures of the lidar data. Additionally improvements in retrieved products as well as advanced products have been developed through integration with observations from other ACTRIS components (e.g. cloud screening from remote sensing clouds component).

The geographical distribution of lidar stations can be found at the EARLINET web site (https://www.earlinet.org/index.php?id=105). Lidar observations in the framework of EARLINET are performed according to a common schedule and on preselected dates. The schedule involves three measurements per week, namely one during daytime at around local noon on Monday at 14:00±1 h and two during nighttime on Monday and Thursday at sunset+2/3 h to enable Raman extinction retrievals. Furthermore, observations are devoted to monitoring special events over the continent, such as Saharan dust outbreaks, forest fires, photochemical smog, and volcanic eruptions (e.g. Balis et al., 2003; Amiridis et al., 2009; Sicard et al., 2011; Pappalardo et al., 2013; Fernández et al., 2018). EARLINET observations have already been used for climatological studies (Amiridis et al., 2005; Giannakaki et al.; 2010; Siomoset al., 2018), long-range transport analysis (Ansmann et al., 2003; Papayannis et al., 2008), aerosol characterization of dust forecast modeling (Perez et al., 2006; Mona et al., 2014), among others. Furthermore, retrieval algorithms related to aerosol microphysical properties were developed with real multi-wavelength lidar data (Müller et al. 2007; Tesche et al, 2009; Balis et al., 2010; Mamouri et al., 2012). So far, EARLINET represents an available tool for validation and exploitation of data from the Cloud-Aerosol Lidar and Infrared Pathfinder Satellite Observation (CALIPSO; Winker et al., 2009) mission and several studies have investigated the CALIPSO products (e.g., Mamouri et al. 2009; Mona et al., 2009; Pappalardo et al. 2010; Amiridis et al., 2015; Papagiannopoulos et al., 2016). Also, the multiwavelength EARLINET data will be very useful for the validation of current and future satellite missions, such as the ESA Explorer missions Atmospheric Dynamics Mission – Aeolus (ADM-Aeolus), Sentinel-5 Precursor (S5-P) Earth Clouds, Aerosols and Radiation Explorer (EarthCARE).

Some of the EARLINET systems perform 24/7 continuous measurements as, for example, the PollyXT systems (Baars et al., 2016; Engelmann et al., 2016). It hence follows that EARLINET consists of rather different lidar systems regarding the number of measured wavelengths and signal channels, the detection range, which is mainly determined by laser power and telescope size and number, the optical design and the electronic signal detection techniques. The majority of EARLINET stations are equipped with multi-wavelength Raman and many of them operate depolarization channels that measure the depolarization of the emitted linearly polarized radiation. In order to ensure qualitative and consistent data processing

https://doi.org/10.5194/acp-2020-601
Preprint. Discussion started: 8 July 2020

Atmospheric Chemistry and Physics Discussions

within the EARLINET network, algorithm intercomparison campaigns have been organized (Matthias et al., 2004; Pappalardo et al., 2004; Böckmann et al., 2004). These campaigns aimed to assure the homogeneity of the data despite the differences in the lidar systems of the stations.

3. Data and Methodology

3.1 Satellite data (GOME-2)

3.1.1 Absorbing Aerosol Index (AAI)

The Absorbing Aerosol Index (AAI) indicates the presence of elevated amounts absorbing aerosols in the Earth's atmosphere. It separates the spectral contrast at two ultraviolet (UV) wavelengths (340/380nm) caused by aerosol scattering and absorption from other effects, including molecular Rayleigh scattering, surface reflection and gaseous absorption (Torres et al., 1998). The aerosol types that are mostly seen in the AAI are desert dust and biomass burning aerosols. Absorbing aerosol index is a unitless parameter, with higher values indicating elevated amount of aerosols present in the atmosphere. Negative values are caused by the presence of clouds and/or scattering aerosol in the scene. However a positive value for the AAI can only be explained by the presence of absorbing aerosols. The Absorbing Aerosol Index (AAI) from GOME-2 is produced by the Royal Netherlands Meteorological Institute, KNMI, -within the framework of the AC SAF. The GOME-2 AAI products are calculated for all three MetOp-A, MetOp-B and MetOp-C satellite instruments and data are available since January 2007, December 2012 and January 2019, respectively (ACSAF: https://acsaf.org/datarecords/aai.html, KNMI: http://www.temis.nl/airpollution/absaai/)

3.1.2 Absorbing Aerosol Height (AAH)

The Absorbing Aerosol Height (AAH) is a new product for aerosol detection, developed by KNMI within the AC SAF. It uses the Absorbing Aerosol Index (AAI) as an indicator to derive the actual height of the absorbing aerosol layer in the O2-A band using the Fast Retrieval Scheme for Clouds Observables (FRESCO) algorithm (Wang et al. 2008, 2012; Tilstra et al., 2012). The retrieved aerosol height varies from the bottom to the top of the aerosol layer, depending on the aerosol optical thickness (AOT), solar zenith angle (SZA) and actual aerosol layer top height (Wang et al., 2008). The AAH product can be used to monitor volcanic eruptions globally and provide the height of the ash layers (Balis et al., 2016). The Absorbing Aerosol Height is very sensitive to cloud contamination. However, aerosols and clouds can prove difficult to distinguish and AAH is computed for different FRESCO cloud fractions. Not only FRESCO is able to determine the height of an absorbing aerosol layer in the absence of clouds, but under certain conditions also in the presence of clouds. Further details and more information associated with AAH product, are available in the Product User Manual (PUM) and Algorithm Theoretical Basis Document (ATBD; Tilstra et al. 2019).

As discussed in the ATDB, observation pixels with AAI values below 2.0 correspond to scenes with too low amount levels of aerosol to result in a reliable AAH retrieval. Also for AAI values larger than 2.0 but smaller than 4.0 the aerosol layer is not in all cases thick enough for a reliable retrieval. However, most of our aerosol cases correspond to AAI values below the 4.0 level. In summary, the AAH algorithm retrieves, from the GOME-2 level-1b Product, the following parameters CF (effective aerosol/cloud fraction), CH (aerosol/cloud height), SA (scene albedo), SH (scene height). Two different

https://doi.org/10.5194/acp-2020-601
Preprint. Discussion started: 8 July 2020

Atmospheric Chemistry and Physics Discussions

aerosol/cloud layer heights (CH and SH) are determined by the AAH algorithm. It is up to the algorithm to decide which of the two is the best candidate to represent the actual AAH level. According to Wang et al. (2012) in order to distinguish whether the contribution of clouds is crucial, three situations about the reliability of the AAH product are used and the effective cloud fraction (CF) is used to check in which of these regimes is the better solution (A: High reliability, B:medium reliability, C:Low reliability). In more detail:

- **Regime A** (CF<=0.25) refers to the situation in which there is either only a low degree of cloud cover or the aerosol optical depth is sufficiently large to compensate the presence of a cloud layer below the aerosol layer. Exceptions are cases with low aerosol amounts, but these scenes were filtered out beforehand by demanding that the AAI must be higher than a threshold AAI value.
- **Regime B** (0.25<CF<0.75) is an intermediate regime and the AAH found this way is likely to underestimate the AAH in some cases, and the reliability attributed to this regime is medium.
- **Regime C** (CF>=0.75) is the situation of a thick cloud layer present in the scene. In this case an aerosol layer is only retrieved successfully when the aerosol layer is sufficiently thick. The reliability is therefore characterized as low. More information can found in Wang et al. (2012)

In the Sect. 3.3, a pie chart (Fig.6) with the distribution of reliability category (Regime) of collocated observations is presented, including the contribution of clouds.

3.2 Ground-based lidar data (EARLINET)

The EARLINET database represents the largest collection of ground-based data of the vertical aerosol distribution on a continental scale. EARLINET members, as well as external users, get access to the database through a web interface (www.earlinet.org; Last access: 23 April 2020). Additionally EARLINET data are permanently indexed and published at WDCC (https://www.earlinet.org/index.php?id=247). The main information stored in the files of the EARLINET database is the vertical distribution backscatter and aerosol extinction coefficients. Additionally, there are more optional variables included in the files, such as the lidar ratio, the particle linear depolarization ratio and the water vapor mixing ratio profiles. In this study we use the backscatter profiles for aerosol layer height retrieval. The backscatter files contain at least a profile of the aerosol backscatter coefficient ($m^{-1}sr^{-1}$) derived from the elastic backscatter signal and may be accompanied by an extinction coefficient profile. Here we use the vertical information of backscatter profiles (at 1064nm and 532nm in some cases) for selected EARLINET stations. Quality assurance (QA) tests have been established and software intercomparison campaigns (Böckmann et al., 2004; Matthias et al., 2004) have been organized in the framework of EARLINET in order to assure the homogeneity of the data despite the differences in the lidar systems of the stations. A list of the EARLINET stations used for the validation of GOME-2 AAH and their geographical coordinates are given in Table 1 and presented in Fig.1. The stations are located such that four European core regions are covered: Central Europe, Western Mediterranean, Central Mediterranean and eastern Mediterranean. In this way, a large variety of aerosol optical and geometrical characteristics can be investigated.

https://doi.org/10.5194/acp-2020-601
Preprint. Discussion started: 8 July 2020

Atmospheric Chemistry and Physics Discussions

3.2.1 Wavelet covariance transform (WCT) method

In this section we analyze the algorithmic processes that are required to extract geometrical features from lidar signals employed in this work. The aerosol geometrical properties carry information about the structure of lidar profiles, such as the boundary layer height and the features of the lofted aerosol layers and can be obtained from any lidar profile. In this study a full lidar dataset from thirteen EARLINET stations has been used for the calculations. Some lidar optical products however are more reliable to use than others. For example, the longer wavelengths typically magnify the differences in the vertical distribution of the aerosol load, resulting in layers that are easier to identify. Furthermore, the Raman inversion always results in profiles that are less structured for the extinction coefficients than the backscatter coefficients. This is the reason why we prioritize them so as to produce geometrical properties. (Baars et al., 2008; Siomos et al., 2017) The product with the highest potential to magnify the layer structure available is selected for each measurement. More specifically, the backscatter products are prioritized over the extinction products, and the longer wavelengths over the shorter ones. For this study, backscatter profiles at 1064nm have been chosen primarily, and in some cases backscatter profiles at 532nm.

Our analysis is based on the method of Baars et al. (2008) that applies the wavelet covariance transform (WCT) to the raw lidar data in order to extract geometrical features such as the PBL height and the cloud boundaries. Many methods have been proposed for the calculation of the PBL height from lidar data (Flamant et al., 1997; Brooks, 2003). The WCT transformation has also been applied successfully in the past on other lidar products. Siomos et al. (2017), for example, use an adaptation of the WCT method and calculate the geometrical features from the aerosol concentration profiles. The wavelet covariance transform was defined as a means of detecting step changes in a signal. It is based upon a compound step function, the Haar function *h*, defined as shown in Eq. (1):

$$h\left(\frac{z-b}{a}\right) = \begin{cases} +1: b-\frac{a}{2} \le z \le b \\ -1: b \le z \le b+\frac{a}{2} \\ 0: elsewhere, \end{cases} \tag{1}$$

Here, h[(z-b)/a] is the Haar function, a is the dilation of the Haar function indicating the size of the window (or dilation), b is the center of the Haar function (or the translation) and z is the altitude range. The covariance transform of the Haar function, $W_f(a, b)$, is defined as shown in Eq. (2):

$$W_f(a,b) = a^{-1} \int_{z_0}^{z_1} f(z)\, h\left(\frac{z-b}{a}\right) dz \tag{2}$$

where $f(z)$ is the backscatter lidar signal, z_b and z_t are the lowest altitude and the highest altitude of possible layers heights. The $W_f(a,b)$ is referred to as the wavelet coefficient. These variables define the window function. Based on the defined lower and upper limits the Haar transform is calculated. The obtained Haar values are subjected to the covariance transform and the maximum negative value of the covariance transform provides the aerosol layer top. The key issues of

https://doi.org/10.5194/acp-2020-601
Preprint. Discussion started: 8 July 2020

Atmospheric Chemistry and Physics Discussions

performing the WCT are the determination of the dilation value of the Haar function. As with previous studies (Brooks et al., 2003; Baars et al., 2008), the dilation factor *a,* affects the number of covariance wavelet transform coefficient local minima. Larger values of dilation factor reveal a few large local minima, at the height of the biggest aerosol loading in the aerosol backscatter profile. In addition, lower dilation values, create local minima at heights of smaller aerosol loads in the profiles. A dilation of 0.5 km is used in this study for the lofted aerosol layer height calculations. An example of a lidar backscatter profile with resulting WCT profile from the Barcelona lidar station (Universitat Politechnica de Catalunya, Barcelona – UPC) on June 29, 2019 is given in Fig.2.

3.3 Validation methodology and collocation criteria

The validation of products with a typical resolution of several kilometers against point-like ground-based measurements involves uncertainties. A key question is how well the ground-based observation represents a larger area around the measurement site and to a large extent depends on the characteristics of the station location (urban, sub-urban, etc). In this study, to obtain a significant number of collocated GOME-2 – EARLINET cases, data from thirteen EARLINET stations were used for the GOME-2 AAH product validation as shown in Table 1. As the UV-VIS satellite instruments provide daytime observations, only the lidar measurements temporally close to the satellite overpass are used in this comparison. The lidar backscatter profiles are used to retrieve aerosol layer height (ALH) information of the aerosol vertical profile, while the AAH product is extracted by the GOME-2 algorithm. For the comparison of GOME-2 AAH against aerosol height from EARLINET lidars, the coincidence criteria are set to a 150 km search radius between the satellite pixel center and the geolocation of the ground-based station. The lidar measurements nearest to the GOME-2 overpass time within a 5 hour temporal interval were selected for every available day of measurement, to ensure a sufficiently large collocation database. It should also be noted that the temporal criterion is enforced since most of the EARLINET lidar observations occur at noon or night while the MetOp orbits are in the morning. For each ground based measurement, only the spatially closest GOME-2 measurements were selected in the comparison study. Furthermore, certain criteria for ensuring the quality and representativeness of the satellite measurements, such as sun glint and AAI values greater than 2 were taken into account. In addition, unconverging pixels with AAH set to be 15 km are also excluded. Table 2 lists the GOME-2 quality-assurance thresholds applied in the EARLINET comparison. Selecting these criteria, the total set of available satellite pixels is quite small. Most of the satellite measurements available from GOME-2 / MetOp refer to cases with AAI between 2 and 4.

Applying all these selection criteria resulted in a total of 272 correlative GOME-2 –EARLINET cases suitable for the comparison study and representativeness of the GOME-2 Level-2 AAH product. However, it quickly became clear that further consideration of the individuality of each sensing instrument is required. A large amount of GOME-2 AAH heights below the 1km level are reported, which in most cases are unlikely to be retrieved from a lidar backscatter profile due the system overlap. This is shown in the 0-1km bin of Fig.3 where the collocations are separated depending on the AAH reported per instrument. It is obvious from Fig.3 that in this height bin, there are limited lidar estimates to compare with GOME-2 and thus we excluded these cases from the comparisons. The backscatter profiles archived in the EARLINET database have a variable height range which typically extends up to 5-6 km where the most of the lidar signals have an

https://doi.org/10.5194/acp-2020-601
Preprint. Discussion started: 8 July 2020

optimal signal-to-noise ratio. Therefore, as can also be seen for the last bar – for heights above 6km- of Fig.3, there are very few cases where the lidars report heights above that altitude.

As a result of this extra restriction in collocation, the number of GOME-2 – EARLINET cases considered in the assessment of the accuracy and representativeness of the GOME-2 AAH are provided in Table 3, including the code name of the EARLINET station used in figures further in the text. Fig.4 (left) shows the distribution of available of collocated cases for each lidar station and in Fig.4 (right) the distribution of all collocations by year. All three GOME-2 instruments are considered in one single satellite data pool. Fig.5 shows the distribution of all collocated layers around each EARLINET station considered (Athens, Barcelona, Belsk, Granada, Évora, Lecce, Limassol, Minsk, Potenza, Sofia, Thessaloniki and Warsaw) while the concentric red circles denote regions of 150 km from the location of these stations. In Fig.6 the distribution of reliability category (Regime) of collocated observations is presented, including the contribution of clouds. The effective cloud fraction (CF) is a primary indicator for the AAH algorithm and is used to check which of these regimes is more reliable for retrieving the AAH. It is clear that most of the collocated cases belong to the high (regime A) and medium (regime B) reliability categories.

4. Results

4.1 GOME-2 & EARLINET comparison statistics

In this section an overall assessment of the GOME-2 retrieved AAH product is given, using the total dataset of GOME-2 – EARLINET collocated cases. Fig.7 is a summary histogram plot showing the distribution of GOME-2 AAH and EARLINET aerosol layer height differences for all EARLINET stations shown in this report for a total of 172 collocated cases. The near Gaussian distribution of the absolute difference is centered slightly to the left, indicating lower GOME-2 AAH values on average with a mean bias of -0.16km and standard deviation of 1.72km, a very promising result considering all the individual uncertainties of both datasets as well as the collocation criteria. The related metrics are given in Table 4. Fig.8 shows the updated bar plot, effectively demonstrating the reason for the lingering differences between the two datasets. A comparison for all study stations can be seen in Fig.9 where the collocations are now colour-coded per their associated AAI value. The overall agreement is quite satisfactory with most lidar AAH values between 1 and 7km, while the GOME-2 AAH results range a bit higher up to ~8km. The individual station statistics are given in Table 6, sorted by the number of collocations found for each station. The mean bias (GOME-2 AAH – EARLINET ALH) falls well within the ±1 km range, with an associated standard deviation between 0.5 and ~2 km. Considering the differences mainly in the temporal collocation and the difference between the satellite pixel size and the point view of the ground-based observations, these results are quite promising as the stable aerosol layers are well captured by the satellite sensors.

Some of the lingering differences may be explained as follows: as per Fig.3, the geometrical and technical characteristics of each lidar system determine the height range where backscatter profiles can be retrieved, and this can affect the comparisons at very low and very high ALHs. Additionally, GOME-2 AAH retrieval assumes a single aerosol layer in the atmospheric column, while it is a common feature to have more layers in the column. This is well captured by the lidar observations, but making the GOME-2 against lidar comparison there is some uncertainty which lidar derived layer should be compared to the GOME-2 equivalent one.

Atmospheric Chemistry and Physics Discussions

4.2. Saharan dust outbreak event between February 21st and 23rd, 2017

An intense Saharan dust episode occurred between the 20st -23rd of February over the Iberian Peninsula. Analysis of the meteorological conditions during this dust event are described in Fernández et al (2018). In this section we present the evolution of the dust outbreak event that was captured by the Évora, Portugal, lidar station between the 21st and the 23rd of February 2017 as well as the GOME-2 AAH observations.

4.2.1 Évora lidar station

This Évora station is located about 100km eastward from the Atlantic west ocean. Due to its geographical location Évora is influenced by different aerosol type namely urban as well as mineral and forest fire aerosol particles. The lidar system here installed (PAOLI-Portable Aerosol and Cloud Lidar), is a multi-wavelength Raman lidar belonging to the Polly^{XT} family (Baars et al., 2016) with high temporal and spatial resolution, operating since September 2009. It is installed at the Évora Atmospheric Science's Observatory (EVASO) and operated by the University of Évora (UE) and the Institute of Earth Sciences (ICT) (38.56°N, -7.91°E, 293 m a.s.l).The equipment includes three elastic channels in the UV-VIS-IR range (355, 532 and 1064nm), two inelastic (Raman) channels (387 and 607nm) and a further (polarization) channel which detects the cross polarized signal at 532 nm. PAOLI is participating both in the EARLINET and the Spanish and Portuguese Aerosol Lidar Network, SPALINET (Sicard et al., 2009 and 2011). The Évora lidar system, being part of EARLINET, has been quality-assured through direct inter-comparisons, both at hardware (Matthias et al., 2004) and algorithm levels (Böckmann et al., 2004; Pappalardo et al., 2004). During daytime, data provided by the Klett technique (Klett, 1981, 1985) use as input a constant lidar ratio value to retrieve the backscatter coefficient values with an average uncertainty of the order of 20–30% (Bösenberg et al., 2003).

4.2.2 Case study: Évora, 21-23 February 2017

In February 2017, an exceptionally extreme event affected the whole Iberian Peninsula, as examined with AERONET, EARLINET lidars and passive-satellite observations (Fernández et al. 2018). MetOp overpasses close to the EARLINET station of Évora are analyzed here to demonstrate the performance of the GOME-2 instrument under intense Saharan dust air masses conditions (see Fig.13). This typical case concerns an intense Saharan dust outbreak, which lasted for three days (21 to 23 February 2017) and was successfully followed during these three days by the Évora lidar station. A combined use of lidar profiles, back-trajectory analysis, dust models and satellite observations allows the identification of Saharan dust cases. Fig.10 shows the temporal evolution of the aerosol total attenuated backscatter coefficient at 1064nm ($m^{-1}sr^{-1}$) over Évora on 21-23 February.

In order to verify the origin of the aerosol layers, observed by the ground-based lidar and GOME-2/MetOp satellite, we calculated backward air-mass trajectories by using the HYSPLIT model (Hybrid Single-Particle Lagrangian Integrated Trajectory, available online at http://ready.arl.noaa.gov/HYSPLIT.php) through the READY system on the site of Air Resource Laboratory, ARL, of NOAA, USA (National Oceanic and Atmospheric Administration) (Stein et al., 2015; Rolph et al., 2017). GDAS (Global Data Analysis System) meteorological files with a spatial resolution of $1^{\circ}\times1^{\circ}$ every 3 h, generated and maintained by ARL, are used as data input. The calculations of backward air mass trajectories show the provenance of the air mass traversed for a chosen time period before arriving at Évora at 10:00 UTC. The temporal evolution of five days backward trajectories, from 21 to 23 February 2017 for arrival heights 1000 (red), 2000 (blue) an 3500 (green) to cover the height range of the observed layers that we recognize in structures of height time displays of the range-corrected lidar signal is shown in Fig.11. The trajectory analysis reveals that the origin of aerosol air masses is indeed the Sahara desert.

In Fig.12, satellite maps from MODIS (Moderate resolution Imaging Spectroradiometer) instrument aboard the Terra satellite, show the dust being transported by air masses over the Atlantic before returning towards Portugal and Spain on the 21st (left), 22nd (middle) and 23rd (right) of February 2017. To illustrate the evaluation methodology for the GOME-2 Level2 Absorbing Aerosol Height, a pair of collocated and concurrent GOME-2 and EARLINET lidar observations is shown in Fig.13. We apply the proposed methodology in the measurement performed at the morning of 23rd of February 2017. The case study was selected as a large set of GOME-2 AAH retrieved pixels is available and extremely high values of Absorbing Aerosol Index (AAI) are observed indicating the large aerosol dust load during this day. The retrieved absorbing aerosol height pixels are shown in Fig.13 (right panel) and the retrieved AAI in Fig.13 (left panel). Data gaps in the maps represent screened-out bright pixels due to either cloud or pixels affected by the sun glint effect while recall that AAH retrievals are only available when AAI is ≥ 2. We will examine this date in particular later on as the extremely high AAI values, as well as the direct temporal morning collocations, give us confidence in the resulting comparisons.

As mentioned above both ground and satellite followed this major dust event for all three days of February 2017. An example of the equivalent backscatter profiles observed by EARLINET station and the information about coincidence of AAH measured by GOME-2 are reported Figure 15. The horizontal dashed blue lines in the left plots column indicate the AAH value derived from the centered GOME-2 pixel. Additional information such as the absorbing aerosol height (AAH), aerosol height error, absorbing aerosol index (AAI), cloud fraction (CF) and distance of collocated centered GOME-2 pixels from EARLINET station are displayed as legend. On the 21st of February, a well-defined aerosol layer is picked up by the lidar at 10:01:23 UT (Fig.14, upper panel, left plot) spanning between 1.5 and 3 km. The collocated GOME-2B observation between 09:59 and 10:30 UTC, at a distance of 62.7 km from the ground station, has an associated AAI value of 2.65, cloud fraction of 10% and an AAH estimate at 2.07 km (blue dashed line), well within the range seen by the lidar at the surface. For the case of the 22nd of February, the aerosol layer appears to split into two separate plumes (Fig.14 middle panel, left plot), with GOME-2A reporting an AAI value of 2.07, i.e. quite close to the threshold value of 2.0. Even though the cloud fraction remains low (~10%), the satellite AAH estimate is quite low (0.8 km). On the 23rd of February, (Fig.14, bottom) GOME-2B reports a pixel quite close to the station, at 25 km, and even though the reported AAH of 2.8 km (dashed blue line) is well within the range of the aerosol layer height reported by the lidar, the high cloud fraction of 45% and associated extreme AAI value of 5.75 makes it difficult to draw further conclusions.

In order to assess whether the general agreement shown by the collocations of Fig.13 can be turned into a generalized comment as to the behavior of the GOME-2 AAH algorithm for cases of high AAI and good temporal collocations, the comparisons for all GOME-2 pixels against the simultaneous lidar observation colour-coded by their associated AAI value is shown in Fig.15. Due to the sufficient amount of collocations in this case study, only observations with AAI larger than 4 are shown. The spread of the satellite estimates are within ±1km from the lidar observations (red and green dashed lines) for the vast majority of the cases shown, for all spatial distances between ground and satellite pixel. The results of this study case could be also interpreted taking into account the representativeness study done using EARLINET and CALIPSO data (Pappalardo et al., 2010) during an intense dust case in 27–30 May 2008. The agreement seems to decrease with larger distances and this follows the losing of correlation between observation when the distance from station increasing. Additionally at the same study, Pappalardo et al. (2010) demonstrate that at 100 km maximum horizontal distance, the variability is strong already with time differences larger than 1 hour, so probably this is the reason of the observed differences between satellite and ground based observations. These results further strengthens our original assessment that the satellite algorithm is mature enough to observe stable and well-spread aerosol layers in the troposphere.

5. Summary and conclusions

In this paper, the first validation of the GOME-2/MetOp absorbing aerosol height (AAH) product against ground-based aerosol layer height (ALH) information, retrieved from the European Aerosol Research Lidar Network, EARLINET, lidar observations of backscatter profiles at 532 nm and 1064nm is presented. The total number of carefully screened collocations with the EARLINET lidar measurements was 172 for the three GOME-2 instruments aboard on MetOpA, MetOpB and MetOpC, between 2007 and 2019. A wide choice of stations around Europe was made in order to examine the behavior of the comparisons for different typical common aerosol load over the locations; South European stations are often affected by Saharan dust intrusions, Central European stations are further affected by local and transboundary pollution events of both anthropogenic and natural origin and Northern European stations are mostly free of dust and most sense particle of anthropogenic provenance. A spatial collocation criterion of 150km, and temporal of 5h, were selected, so as to obtain a sufficient amount of collocations. The official lidar EARLINET dataset has been post-reprocessed by an automatic geometrical features detection algorithm, known as the WCT algorithm. The WCT method make uses of the elastic backscattered coefficient at 532 and 1064nm in combination with criteria flags. This method can be only applied in stations with at least one elastically resolved backscatter profile. The results of this article encourages the operational usage of the WCT-based algorithms in validation processes. The inter-comparison results are very promising, showing that the GOME-2 AAH measurements provide a good estimation of the aerosol layer altitudes sensed by the lidar ground-based instruments. On average, the mean absolute bias (GOME2 minus lidar height) was found to be -0.16±1.72km, with a near Gaussian distribution and minimum and maximum differences between ~ ±5km. On a station-basis, and with a couple of exceptions, their mean biases fall in the ±1 km range with an associated standard deviation between 0.5 and 2 km. Considering the differences, mainly due to the temporal collocation and the difference between the satellite pixel size and the point view of the ground-based observations, these results are quite promising and demonstrate that stable aerosol layers are well captured by the satellite sensors. The official AC SAF requirements on the accuracy of the GOME-2 AAH product state that, for heights < 10 km, the threshold accuracy is 3km, the target accuracy is 2km and the optimal accuracy is 1 km. This validation effort shows that for all cases the target accuracy is achieved, and for specific aerosol heights, also the optimal, well within user requirements.

An extreme Saharan dust event, which advected large dust loads from the North African continent over Iberian Peninsula on February 21st to 23rd, 2017, was analyzed in detailed. In this case, numerous collocations were found within ±30min with

https://doi.org/10.5194/acp-2020-601
Preprint. Discussion started: 8 July 2020

the Évora, Portugal, lidar system. This permitted a more stringent criterion on the Absorbing Aerosol Index, AAI, to be used, permitting collocations with associated AAI > 4 to be considered. For this well-developed and spatially well-spread aerosol layer, most GOME-2 retrievals fall within 1km of the temporally collocated lidar observation for the entire range of 0 to 150km radius permitted. This finding further testifies to the capabilities of the MetOp-born instruments to sense the atmospheric aerosol layer height. EARLINET represents an optimal tool to validate satellite instruments data and to provide necessary information to fully exploit the data produced. Furthermore, the EARLINET network is a suitable database to contribute also to future passive satellite missions such as TROPOMI S5P (http://www.tropomi.eu/) for the validation of aerosol layer height products.

Data availability. The data of the GOME-2 Absorbing Aerosol Height (AAH) product are provided by KNMI in the framework of the EUMETSAT Satellite Application Facility on Atmospheric Composition Monitoring (AC SAF). GOME-2 AAI browsed images are freely distributed via the TEMIS website at http://www.temis.nl. EARLINET aerosol profile data are reported in the EARLINET Data base: https://data.earlinet.org, and are accessible from its repository and from the ACTRIS Data Portal (http://actris.nilu.no). The data policy of these data is harmonized with the ACTRIS data policy. The authors gratefully acknowledge the NOAA Air Resources Laboratory (ARL) for the provision of the HYSPLIT transport and dispersion model and/or READY website https://www.ready.noaa.gov used in this publication.

Acknowledgments.The authors would like to thank the teams responsible for the provision of satellite and ground-based data used in this paper. The data of the GOME-2 Absorbing Aerosol Index are provided by KNMI in framework of the EUMETSAT Satellite Application Facility on Atmospheric Composition (AC SAF). The authors acknowledge EARLINET for providing aerosol lidar profiles available at https://data.earlinet.org/. We further acknowledge the support of this work by the project "PANhellenic infrastructure for Atmospheric Composition and climatE change" (MIS 5021516) which is implemented under the Action "Reinforcement of the Research and Innovation Infrastructure", funded by the Operational Programme "Competitiveness, Entrepreneurship and Innovation" (NSRF 2014-2020) and co-financed by Greece and the European Union (European Regional Development Fund). The work is partially supported by the ACTRIS-2 project, funded from the European Union's Horizon 2020 research and innovation programme (grant agreement No. 654109) and by ACTRIS-IMP (Implementation project), funded in the frame of the programme H2020 Grant Agreement 871115. The work is partially supported by the European Union through the European Regional Development Fund, included in the COMPETE 2020 (Operational Program Competitiveness and Internationalization) through the ICT project (UIDB/04683/2020) with the reference POCI-01-0145- FEDER-007690 and also through TOMAQAPA (PTDC/CTAMET/ 29678/2017)

https://doi.org/10.5194/acp-2020-601
Preprint. Discussion started: 8 July 2020

Atmospheric Chemistry and Physics Discussions

References

Amiridis, V., Balis, D., Kazadzis, S., Bais, A., Giannakaki, E., Papayannis, A., and Zerefos, C.: Four years aerosol observations with a Raman lidar at Thessaloniki, Greece in the framework of EARLINET, J. Geophys. Res., 110, D21203,doi:10.1029/2005JD006190, 2005.

Amiridis, V., Balis, D. S., Giannakaki, E., Stohl, A., Kazadzis, S., Koukouli, M. E., and Zanis, P.: Optical characteristics of biomass burning aerosols over Southeastern Europe determined from UV-Raman lidar measurements, Atmos. Chem. Phys., 9, 2431–2440, doi:10.5194/acp-9-2431-2009, 2009.

Amiridis, V., E. Marinou, A. Tsekeri, U. Wandinger, A. Schwarz, E. Giannakaki, R. Mamouri, P. Kokkalis, I. Binietoglou, S. Solomos, T. Herekakis, S. Kazadzis, E. Gerasopoulos, D. Balis, A. Papayannis, C. Kontoes, K. Kourtidis, N. Papagiannopoulos, L. Mona, G. Pappalardo, O. Le Rille, and A. Ansmann: LIVAS: a 3-D multi-wavelength aerosol/cloud climatology based on CALIPSO and EARLINET, Atmos. Chem. Phys., 15, 7127-7153, doi:10.5194/acp-15-7127-2015, 2015

Ansmann, A., et al., Long-range transport of Saharan dust to northern Europe: The 11 – 16 October 2001 outbreak observed with EARLINET,J. Geophys. Res.,108(D24), 4783, doi:10.1029/2003JD003757, 2003

Baars, H., Ansmann, A., Engelmann, R., and Althausen, D.: Continuous monitoring of the boundary-layer top with lidar, Atmos. Chem. Phys., 8, 7281–7296, https://doi.org/10.5194/acp-8-7281-2008, 2008.

Baars, H., Kanitz, T., Engelmann, R., Althausen, D., Heese,B., Komppula, M., Preißler, J., Tesche, M., Ansmann, A.,Wandinger, U., Lim, J.-H., Ahn, J. Y., Stachlewska, I. S.,Amiridis, V., Marinou, E., Seifert, P., Hofer, J., Skupin, A.,Schneider, F., Bohlmann, S., Foth, A., Bley, S., Pfüller, A., Giannakaki, E., Lihavainen, H., Viisanen, Y., Hooda, R. K., Pereira, S. N., Bortoli, D., Wagner, F., Mattis, I., Janicka, L., Markowicz, K. M., Achtert, P., Artaxo, P., Pauliquevis, T., Souza, R. A. F.,Sharma, V. P., van Zyl, P. G., Beukes, J. P., Sun, J., Rohwer, E. G.,Deng, R., Mamouri, R.-E., and Zamorano, F.: An overview of the first decade of PollyNET: an emerging network of automated Raman-polarization lidars for continuous aerosol profiling, Atmos. Chem. Phys., 16, 5111–5137, https://doi.org/10.5194/acp-16-5111-2016, 2016.

Balis D.S, V. Amiridis, C. Zerefos, E. Gerasopoulos, M. Andreae, P. Zanis, A. Kazantzidis, S. Kazadzis and A. Papayannis, Raman lidar and sunphotometric measurements of aerosol optical properties over Thessaloniki, Greece during a biomass burning episode, Atm. Env., 37,32, 4529-4538, 2003.

Balis D., E. Giannakaki, D. Müller, V. Amiridis, K. Kelektsoglou, S. Rapsomanikis and A. Bais, Estimation of the microphysical aerosol properties over Thessaloniki, Greece, during the SCOUT-O3 campaign with the synergy of Raman lidar and sunphotometer data, J. of Geophys. Res., 115, D08202, doi:10.1029/2009JD013088, 2010.

Balis, D., Koukouli, M.-E., Siomos, N., Dimopoulos, S., Mona,L., Pappalardo, G., Marenco, F., Clarisse, L., Ventress, L. J.,Carboni, E., Grainger, R. G., Wang, P., Tilstra, G., van der A,R., Theys, N., and Zehner, C.: Validation of ash optical depthand layer height retrieved from passive satellite sensors using EARLINET and airborne lidar data: the case of the Eyjafjallajökull eruption, Atmos. Chem. Phys., 16, 5705–5720, https://doi.org/10.5194/acp-16-5705-2016, 2016.

Böckmann, C., Wandinger, U., Ansmann, A., Bösenberg, J.,Amiridis, V., Boselli, A., Delaval, A., De Tomasi, F., Frioud,M., Grigorov, I., Hagard, A., Horvat, M., Iarlori, M., Komguem,L., Kreipl, S., Larcheveque, G., Matthias, V.,

https://doi.org/10.5194/acp-2020-601
Preprint. Discussion started: 8 July 2020

Papayannis, A.,Pappalardo, G., Rocadenbosch, F., Rodrigues, J. A., Schneider,J., Shcherbakov, V., and Wiegner, M.: Aerosol lidar intercomparison in the framework of the EARLINET project: Part II –Aerosol backscatter algorithms, Appl. Opt., 43, 977–989, 2004.

Brooks, I.M.: Finding Boundary Layer Top: Application of a Wavelet Covariance Transform to Lidar Backscatter Profiles, J. Atmos.Ocean.Tech.,20,1092–1105, https://doi.org/10.1175/1520-0426(2003)020<1092:FBLTAO>2.0.CO;2, 2003.

Engelmann, R., Kanitz, T., Baars, H., Heese, B., Althausen, D.,Skupin, A., Wandinger, U., Komppula, M., Stachlewska, I. S.,Amiridis, V., Marinou, E., Mattis, I., Linné, H., and Ansmann,A.: The automated multiwavelength Raman polarization and water-vapor lidar PollyXT: the neXT generation, Atmos. Meas. Tech., 9, 1767–1784, doi:10.5194/amt-9-1767-2016, 2016

Fernández, A. J., Sicard, M., Costa, M. J., Guerrero-Rascado, J. L., Gómez-Amo, J. L., Molero, F., Barragán, R., Bortoli, D., Bedoya-Velásquez, A. E., Utrillas, M. P., Salvador, P., Granados-Muñoz, M. J., Potes, M., Ortiz-Amezcua, P., Martínez-Lozano, J. A., Artíñano, B., Muñoz-Porcar, C., Salgado, R., Román, R., Rocadenbosch, F., Salgueiro, V., Benavent-Oltra, J. A., Rodríguez-Gómez, A., Alados-Arboledas, L., Comerón, A., and Pujadas, M.: February 2017 extreme Saharan dust outbreak in the Iberian Peninsula: from lidar-derived optical properties to evaluation of forecast models, Atmos. Chem. Phys. Discuss., https://doi.org/10.5194/acp-2018-370, 2018.

Flamant, C., J. Pelon, P. H. Flamant, and P. Durand Lidar determination of the entrainment zone thickness at the top of the unstable marine atmospheric boundary layer. Bound. Layer Meteor., 83, 247–284, 1997

Giannakaki, E., Balis, D. S., Amiridis, V., and Zerefos, C.: Optical properties of different aerosol types: seven years of combined Raman-elastic backscatter lidar measurements in Thessaloniki, Greece, Atmos. Meas. Tech., 3, 569–578, https://doi.org/10.5194/amt-3-569-2010, 2010.

Hassinen, S., Balis, D., Bauer, H., Begoin, M., Delcloo, A., Eleftheratos, K., Gimeno Garcia, S., Granville, J., Grossi, M., Hao, N.,Hedelt, P., Hendrick, F., Hess, M., Heue, K.-P., Hovila, J., Jønch-Sørensen, H., Kalakoski, N., Kauppi, A., Kiemle, S., Kins, L.,Koukouli, M. E., Kujanpää, J., Lambert, J.-C., Lang, R., Lerot,C., Loyola, D., Pedergnana, M., Pinardi, G., Romahn, F., van Roozendael, M., Lutz, R., De Smedt, I., Stammes, P., Steinbrecht, W., Tamminen, J., Theys, N., Tilstra, L. G., Tuinder, O.N. E., Valks, P., Zerefos, C., Zimmer, W., and Zyrichidou, I.:Overview of the O3M SAF GOME-2 operational atmospheric composition and UV radiation data products and data availability, Atmos. Meas. Tech., 9, 383–407, doi:10.5194/amt-9-383-2016, 2016

IPCC 2013: Climate Change 2013: The Physical Science Ba-sis, Contribution of Working Group I to the Fifth Assessment Report of the Intergovernmental Panel on Climate Change,edited by: Stocker, T. F., Qin, D., Plattner, G. K., Tignor,M., Allen, S. K., Boschung, J., Nauels, A., Xia, Y., Bex,V., and Midgley, P. M., Cambridge University Press, Cambridge, United Kingdom and New York, NY, USA, 1535 pp.,https://doi.org/10.1017/CBO9781107415324.

Klett, J.D.: Stable analytical inversion solution for processing lidar returns, Appl. Opt., 20, 211–220, https://doi.org/10.1364/AO.20.000211, 1981.

Klett, J. D.: Stable analytic inversion solution for processing lidar returns, Appl. Optics, 20, 211–220, 1981.Klett, J. D.: Lidar inversion with variable backscatter/extinction ratios, Appl. Optics, 24, 1638–1643, 1985.

Mamouri, R. E., Papayannis, A., Amiridis, V., Müller, D., Kokkalis,P., Rapsomanikis, S., Karageorgos, E. T., Tsaknakis, G., Nenes,A., Kazadzis, S., and Remoundaki, E.: Multi-wavelength Raman lidar, sun photometric and aircraft

https://doi.org/10.5194/acp-2020-601
Preprint. Discussion started: 8 July 2020

Atmospheric Chemistry and Physics
Discussions

measurements in combination with inversion models for the estimation of the aerosol optical and physico-chemical properties over Athens, Greece, At-mos. Meas. Tech., 5, 1793–1808, doi:10.5194/amt-5-1793-2012, 2012

Matthias, V., Freudenthaler, V., Amodeo, A., Balin, I., Balis, D.,Bösenberg, J., Chaikovsky, A., Chourdakis, G., Comeron, A., Delaval, A., Tomasi, F. D., Eixmann, R., Hågård, A., Komguem,L., Kreipl, S., Matthey, R., Rizi, V., Rodrigues, J. A., Wandinger,U., and Wang, X.: Aerosol lidar intercomparison in the framework of the EARLINET project. 1.Instruments, Appl. Opt., 43,961–976, https://doi.org/10.1364/AO.43.000961, 2004

Mona, L., Pappalardo, G., Amodeo, A., D'Amico, G., Madonna, F., Boselli, A., Giunta, A., Russo, F., and Cuomo, V.: One year of CNR-IMAA multi-wavelength Raman lidar measurements in coincidence with CALIPSO overpasses: Level 1 products comparison, Atmos. Chem. Phys., 9, 7213–7228, https://doi.org/10.5194/acp-9-7213-2009, 2009.

Mona, L., Papagiannopoulos, N., Basart, S., Baldasano, J., Binietoglou, I., Cornacchia, C., and Pappalardo, G.: EARLINET dust observations vs. BSC-DREAM8b modeled profiles: 12-year-long systematic comparison at Potenza, Italy, Atmos. Chem. Phys., 14, 8781–8793, https://doi.org/10.5194/acp-14-8781-2014, 2014.

Müller, D., Ansmann, A., Mattis, I., Tesche, M., Wandinger, U.,Althausen, D., and Pisani, G.: Aerosol-type-dependent lidar ratios observed with Raman lidar, J. Geophys. Res.-Atmos., 112,D16202, https://doi.org/10.1029/2006JD008292, 2007.

Munro, R., Lang, R., Klaes, D., Poli, G., Retscher, C., Lindstrot, R., Huckle, R., Lacan, A., Grzegorski, M., Holdak, A., Kokhanovsky, A., Livschitz, J., and Eisinger, M.: The GOME-2 instrument on the Metop series of satellites: instrument design, calibration, and level 1 data processing – an overview, Atmos. Meas. Tech., 9, 1279–1301, https://doi.org/10.5194/amt-9-1279-2016, 2016

Papagiannopoulos, N., Mona, L., Alados-Arboledas, L., Amiridis, V., Baars, H., Binietoglou, I., Bortoli, D., D'Amico, G., Giunta, A., Guerrero-Rascado, J. L., Schwarz, A., Pereira, S., Spinelli, N., Wandinger, U., Wang, X., and Pappalardo, G.: CALIPSO climatological products: evaluation and suggestions from EARLINET, Atmos. Chem.

Papayannis, A., Amiridis, V., Mona, L., Tsaknakis, G., Balis, D.,B ̈osenberg, J., Chaikovski, A., De Tomasi, F., Grigorov, I., Mattis, I., Mitev, V., Müller, D., Nickovic, S., Perez, C., Pietruczuk, A., Pisani, G., Ravetta, F., Rizi, V., Sicard, M., Trickl, T., Wiegner, M., Gerding, M., Mamouri, R.E., D’Amico, G., and Pappalardo, G.: Systematic lidar observations of Saharan dust over Europe in the frame of EARLINET (2000–2002), J. Geophys. Res., 113, D10204, doi:10.1029/2007JD009028, 2008.

Pappalardo, G., Amodeo, A., Pandolfi, M., Wandinger, U., Ansmann, A., Bösenberg, J., Matthias, V., Amiridis, V., De Tomasi,F., Frioud, M., Iarlori, M., Komguem, L., Papayannis, A., Rocadenbosch, F., and Wang, X.: Aerosol lidar intercomparison in the framework of the EARLINET project. 3. Raman lidar algorithm for aerosol extinction, backscatter and lidar ratio, Appl. Optics, 43, 5370–5385, 2004

Pappalardo, G., Wandinger, U., Mona, L., Hiebsch, A., Mattis, I., Amodeo, A., Ansmann, A., Seifert, P., Linné, H., Apitu ley, A.,Alados Arboledas, L., Balis, D., Chaikovsky, A., D’Amico, G.,De Tomasi, F., Freudenthaler, V., Gian nakaki, E., Giunta, A.,Grigorov, I., Iarlori, M., Madonna, F., Mamouri, R., Nasti, L.,Papayannis, A., Pietruczuk, A., Pujadas, M., Rizi, V., Roca-denbosch, F., Russo, F., Schnell, F., Spinelli, N., Wang, X.,and Wiegner, M.: EAR LINET correlative measurements forCALIPSO: first intercomparison results, J. Geophys. Res., 115,D00H19, doi:10.1029/2009JD012147, 2010

Pappalardo, G., Mona, L., D'Amico, G., Wandinger, U., Adam, M., Amodeo, A., Ansmann, A., Apituley, A., Alados Arboledas, L.,Balis, D., Boselli, A., Bravo-Aranda, J. A., Chaikovsky, A., Comeron, A., Cuesta, J., De Tomasi, F., Freudenthaler, V., Gausa,M., Giannakaki, E., Giehl, H., Giunta, A., Grigorov, I., Groß, S., Haeffelin, M., Hiebsch, A., Iarlori, M., Lange, D., Linné, H., Madonna, F., Mattis, I., Mamouri, R.-E., McAuliffe, M. A. P.,Mitev, V., Molero, F., Navas-Guzman, F., Nicolae, D., Papayannis, A., Perrone, M. R., Pietras, C., Pietruczuk, A., Pisani, G.,Preißler, J., Pujadas, M., Rizi, V., Ruth, A. A., Schmidt, J.,Schnell, F., Seifert, P., Serikov, I., Sicard, M., Simeonov, V., Spinelli, N., Stebel, K., Tesche, M., Trickl, T., Wang, X., Wagner, F., Wiegner, M., and Wilson, K. M.: Four-dimensional distribution of the 2010 Eyjafjallajökull volcanic cloud over Europe observed by EARLINET, Atmos. Chem. Phys., 13, 4429–4450, https://doi.org/10.5194/acp-13-4429-2013, 2013.

Pappalardo, G., Amodeo, A., Apituley, A., Comeron, A., Freudenthaler, V., Linné, H., Ansmann, A., Bösenberg, J., D'Amico,G., Mattis, I., Mona, L., Wandinger, U., Amiridis, V., Alados-Arboledas, L., Nicolae, D., and Wiegner, M.: EARLINET: towards an advanced sustainable European aerosol lidar network,Atmos. Meas. Tech., 7, 2389–2409, https://doi.org/10.5194/amt-7-2389-2014, 2014.

Pérez, C., Nickovic, S., Baldasano, J. M., Sicard, M., Rocadenbosch, F., and Cachorro, V. E.: A long Saharan dust event over the western Mediterranean: lidar, Sun photometer observations, and regional dust modeling?, J. Geophys. Res., 111, D15214, doi:10.1029/2005JD006579, 2006

Rodríguez-Navarro, C., di Lorenzo, F., Elert, K., 2018. Mineralogy and physicochemical features of Saharan dust wet deposited in the Iberian Peninsula during an extreme red rain event. Atmos. Chem. Phys. 18, 10089–10122. https://doi.org/10.5194/acp-18-10089-2018, 2018

Rolph, G., Stein, A., and Stunder, B., (2017). Real-time Environmental Applications and Display sYstem: READY. Envi ronmental Modelling & Software, 95, 210-28, https://doi.org/10.1016/j.envsoft.2017.06.025, 2017

Sicard, M., Molero, F., Guerrero-Rascado, J. L., Pedros, R., Exposito, F. J., Cordoba-Jabonero, C., Boların, J. M., Comer on, A., Rocadenbosch, F., Pujadas, M., Alados-Arboledas, L., Martinez-Lozano, J. A., Dıaz, J. P., Gil, M., Requena, A., Navas-Guzman, F., and Moreno, J. M.: Aerosol lidar intercomparison in the framework of SPALINET – the SPAnish LIdar NETwork: methodology and results, IEEE Trans. Geosci. Remote Sens.,47, 3547–3559, 2009.

Sicard, M., Pujadas, M., Alados-Arboledas, L., Pedros, R., Dıaz, J. P., Cordoba-Jabonero, C., Requena, A., Comeron, A., Rocadenbosch, F., Wagner, F., Rodrigues, J., Moreno, J. M.: SPALINET: The Spanish and Portuguese aerosol lidar network, Opt. Pura Appl., 44, 1–5, 2011

Siomos, N., Balis, D. S., Voudouri, K. A., Giannakaki, E., Filioglou, M., Amiridis, V., Papayannis, A., and Fragkos, K.: Are EARLINET and AERONET climatologies consistent? The case of Thessaloniki, Greece, Atmos. Chem. Phys., 18, 11885–11903, https://doi.org/10.5194/acp-18-11885-2018, 2018.

Siomos, N., Balis, D. S., Poupkou, A., Liora, N., Dimopoulos, S., Melas, D., Giannakaki, E., Filioglou, M., Basart, S., and Chaikovsky, A.: Investigating the quality of modeled aerosol profiles based on combined lidar and sunphotometer data, Atmos. Chem. Phys., 17, 7003–7023, https://doi.org/10.5194/acp-17-7003-2017, 2017.

Stammes, P., M. Sneep, J. F. de Haan, J. P. Veefkind, P. Wang, and P. F. Levelt , Effective cloud fractions from the Ozone Monitoring Instrument: Theoretical framework and validation, J. Geophys. Res., 113, D16S38, doi:10.1029/2007JD008820, 2008

Stein, A.F., Draxler, R.R, Rolph, G.D., Stunder, B.J.B., Cohen, M.D., and Ngan, F.. NOAA's HYSPLIT atmospheric trans port and dispersion modeling system, Bull. Amer. Meteor. Soc., 96, 2059-2077, http://dx.doi.org/10.1175/BAMS-D-14-00110.1, 2015

Tesche, M., Müller, D., Ansmann, A., Hu, M., Zhang, Y. H. Retrieval of microphysical properties of aerosol particles from one-wavelength Raman lidar and multiwavelength Sun photometer observations, Atmos. Env., 42, 6398-6404, https://doi.org/10.1016/j.atmosenv.2008.02.014, 2008

Tilstra, L. G., M. de Graaf, I. Aben, and P. Stammes, In-flight degradation correction of SCIAMACHY UV reflectances and Absorbing Aerosol Index, J. Geophys. Res., 117, D06209, doi: 10.1029/2011JD016957, 2012

Tilstra, L. G., Wang, P. and Stammes, P.: ALGORITHM THEORETICAL GOME-2 Absorbing Aerosol Height, Royal Netherlands Meteorological Institute, de Bilt, 32 pp., 2019.

Torres, O., Bhartia, P. K., Herman, J. R., Ahmad, Z. and Gleason, J.: Derivation of aerosol properties from satellite measurements of backscattered ultraviolet radiation: Theoretical basis, J. Geophys. Res. Atmos., 103(D14), 17099–17110, doi:10.1029/98JD00900, 1998

Wang, P., Stammes, P.,Van Der A, R., Pinardi, G. and Van Roozendael, M.: FRESCO+: An improved O2A-band cloud retrieval algorithm for tropospheric trace gas retrievals, Atmos. Chem. Phys., 8(21), 6565–6576, doi:10.5194/acp-8-6565-2008, 2008

Wang, P., Tuinder, O. N. E., Tilstra, L. G., De Graaf, M. and Stammes, P.: Interpretation of FRESCO cloud retrievals in case of absorbing aerosol events, Atmos. Chem. Phys., 12(19), 9057–9077, doi:10.5194/acp-12-9057-2012, 2012

Winker, D. M., Vaughan, M. A., Omar, A., Hu, Y., Powell, K. A., Liu, Z., Hunt, W. H. and Young, S. A.: Overview of the CALIPSO mission and CALIOP data processing algorithms, J. Atmos. Ocean. Technol., 26(11), 2310–2323, doi:10.1175/2009JTECHA1281.1, 2009.

https://doi.org/10.5194/acp-2020-601
Preprint. Discussion started: 8 July 2020

Table 1. Summary of the GOME-2 instrument main characteristics (*) GOME-2A tandem operation since 15 July 2013

Instrument / Characteristics	**GOME-2 MetOp-A**	**GOME-2 MetOp-B**	**GOME-2 MetOp-C**
Launch date	19 Oct 2006	17 Sep 2012	7 Nov 2018
Spectral Coverage	240 - 790 nm	240 - 790 nm	240 - 790 nm
Spectral resolution	0.26 - 0.51nm	0.26 - 0.51nm	0.26 - 0.51nm
Spatial Coverage	80 x 40 km 40 x 40 km (*)	80 x 40 km	80 x 40 km
Swath width	1920 km – 960 km	1920 km	1920 km
Equator Crossing Time	09:30 a.m. LT	09:30 a.m. LT	09:30 a.m. LT
Global coverage	3 days (High Res.) 1.5 days (Low Res.)	3 days (High Res.) 1.5 days (Low Res.)	3 days (High Res.) 1.5 days (Low Res.)

https://doi.org/10.5194/acp-2020-601
Preprint. Discussion started: 8 July 2020

Table 2. Locations of EARLINET lidar stations and their geographical coordinates

Site	EARLINET code	Altitude a.s.l (m)	Latitude (°N)	Longitude (°E)
Barcelona, Spain	**BRC**	115	41.39	2.11
Granada, Spain	**GRA**	680	37.16	-3.60
Évora, Portugal	**EVO**	293	38.56	-7.91
Thessaloniki, Greece	**THE**	60	40.63	22.95
Athens, Greece	**ATZ**	212	37.96	23.78
Minsk, Belarus	**MAS**	200	53.91	27.60
Bucharest, Romania	**INO**	93	44.34	26.03
Limassol, Cyprus	**LIM**	10	34.67	33.04
Lecce, Italy	**SAL**	30	40.33	18.10
Potenza, Italy	**POT**	760	40.60	15.72
Sofia, Bulgaria	**SOF**	550	42.65	23.38
Warsaw, Poland	**WAW**	112	52.21	20.98
Belsk, Poland	**COG**	180	51.83	20.78

Table 3. List of GOME-2 quality-assurance thresholds applied in the EARLINET comparison

Absorbing Aerosol Index (AAI)	≥ 2
Sunglint effect	Use only flag values 0, 1, 4, 8, and 33–63 Do not use flag values 32 or 64 and higher
Spatial criterion	≤150 km radius from the EARLINET stations
Temporal window	5 hours

Atmospheric Chemistry and Physics Discussions
Open Access
EGU

Table 4. GOME-2/MetOp and EARLINET cases considered in the validation process

Station	EARLINET code	Common cases
Athens	**ATZ**	3
Barcelona	**BRC**	32
Belsk	**COG**	26
Bucharest	**INO**	10
Évora	**EVO**	5
Granada	**GRA**	32
Lecce	**SAL**	18
Limassol	**LIM**	11
Minsk	**MAS**	5
Potenza	**POT**	2
Sofia	**SOF**	1
Thessaloniki	**THE**	24
Warsaw	**WAW**	3

Table 5. Statistical metrics from the validation between GOME-2 AAH and EARLINET retrieved aerosol layer height

Metric	
Number of collocated cases (no.)	172
Mean difference	-0.18 km
Standard deviation	1.68 km
Min | Max of the differences	-4.91|3.91 km
Median	-0.15 km

https://doi.org/10.5194/acp-2020-601
Preprint. Discussion started: 8 July 2020

Atmospheric Chemistry and Physics Discussions

Table 6. Summary of statistics for the comparisons between GOME-2 AAH and LIDAR ALH for all stations* sorted by maximum number of collocations found.

EARLINET Station	Statistical parameters [in km]				
	N	Mean absolute Bias	STD	Min	Max
Barcelona	32	**-0.35**	**1.94**	**-4.66**	**2.86**
Granada	32	**-0.63**	**1.79**	**-3.65**	**3.9**
Thessaloniki	24	**-0.05**	**1.84**	**-4.71**	**3.24**
Belsk	26	**0.19**	**1.52**	**-3.11**	**3.24**
Lecce	18	**-0.24**	**1.14**	**-3.47**	**2.05**
Bucharest	10	**-0.39**	**1.26**	**-0.96**	**2.96**
Limassol	11	**-0.06**	**1.64**	**-2.89**	**2.80**
Évora	5	**-0.07**	**1.95**	**-1.64**	**3.31**
Minsk	5	**0.56**	**0.61**	**-0.05**	**1.51**
Athens	3	**-2**	**1.38**	**-3.6**	**-1.06**
Warsaw	3	**1.66**	**0.53**	**1.08**	**2.15**
Potenza	2	**-1.4**	**1.1**	-0.64	**-0.64**

***The station of Sofia has only one collocation.**

https://doi.org/10.5194/acp-2020-601
Preprint. Discussion started: 8 July 2020

Atmospheric Chemistry and Physics Discussions

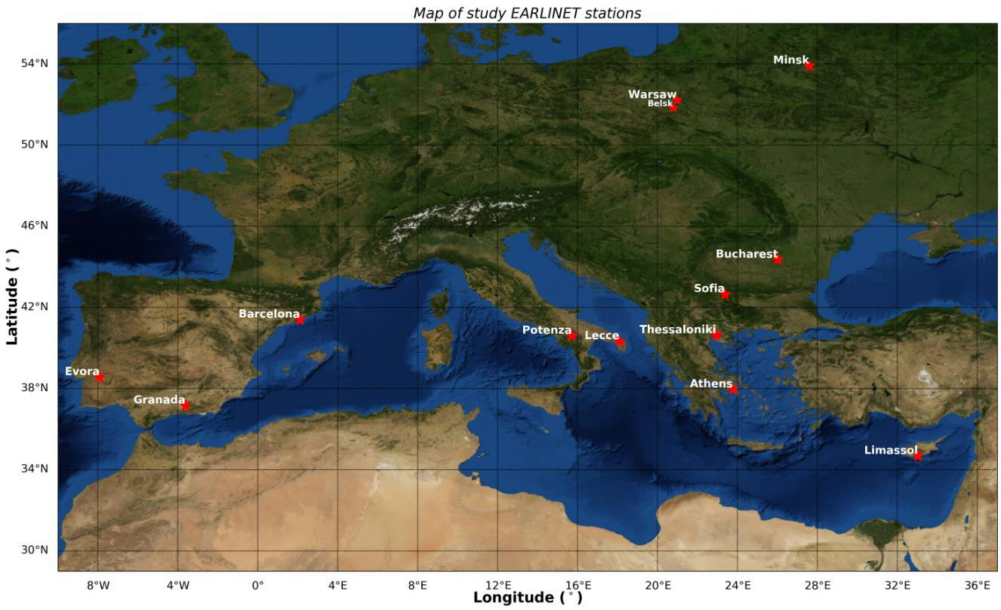

Figure 1. Geographical distributionof EARLINET lidar stations used in this study.

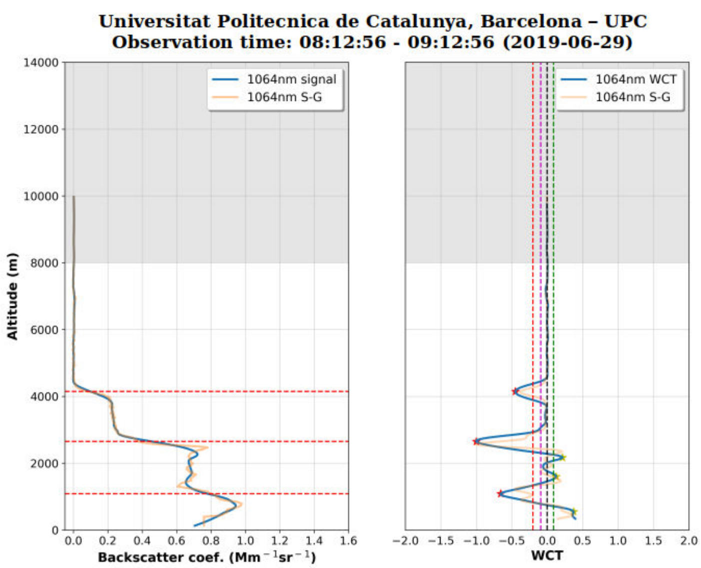

Figure 2. (Left) Lidar backscatter profile at 1064nm and (right) resulting WCT profile from the Barcelona lidar station (Universitat Politechnica de Catalunya, Barcelona – UPC) on June 29, 2019.The label "S-G" indicates that a Savitzky-Golay filter was used to reduce to noise variance in the backscatter profile.

https://doi.org/10.5194/acp-2020-601
Preprint. Discussion started: 8 July 2020

Atmospheric Chemistry and Physics
Discussions

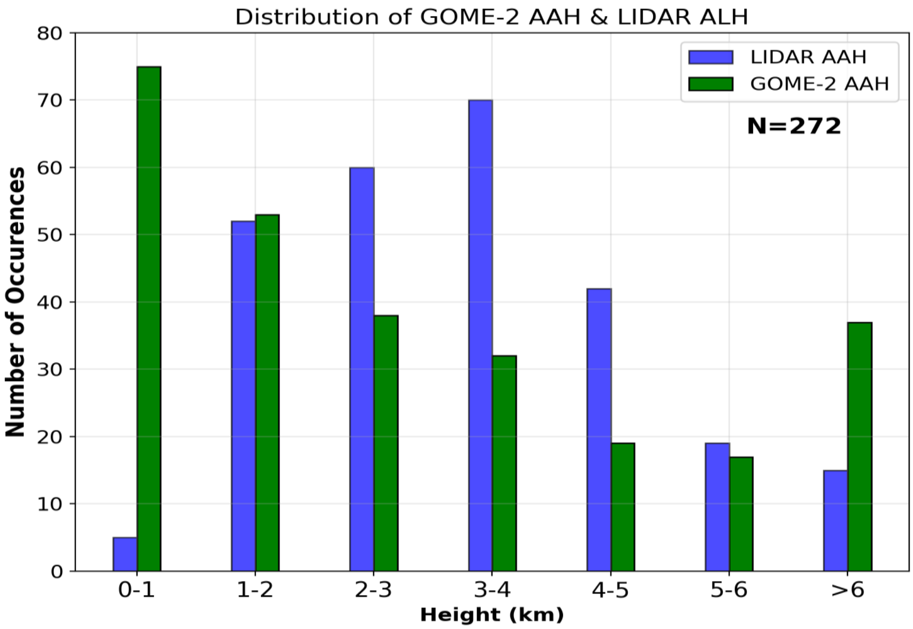

Figure 3. Bar plot of GOME-2 AAH (green) and EARLINET ALH (blue) stations. The height ranges of bins are between 0–1, 1–2, 2–3, 3–4, 4–5, 5-6 and > 6 km. The bar counts indicate the number of collocated cases.

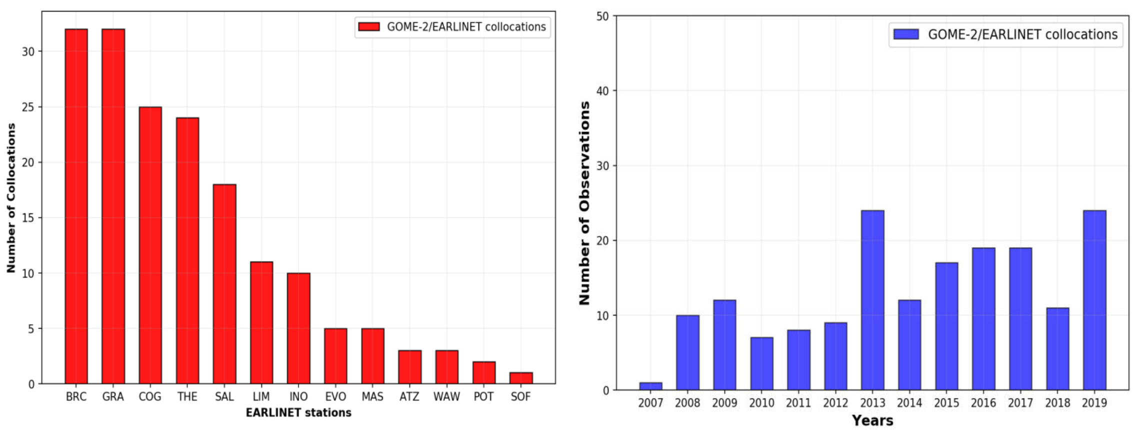

Figure 4. (left) Distribution of collocated cases with minimum distance from each lidar station, for a radius distance 150km around each EARLINET station and (right) distribution of all collocated cases by year for the study period (2007-2019). Refer to Table 4, for the EARLINET code names shown in the x-axis.

https://doi.org/10.5194/acp-2020-601
Preprint. Discussion started: 8 July 2020

Atmospheric Chemistry and Physics Discussions

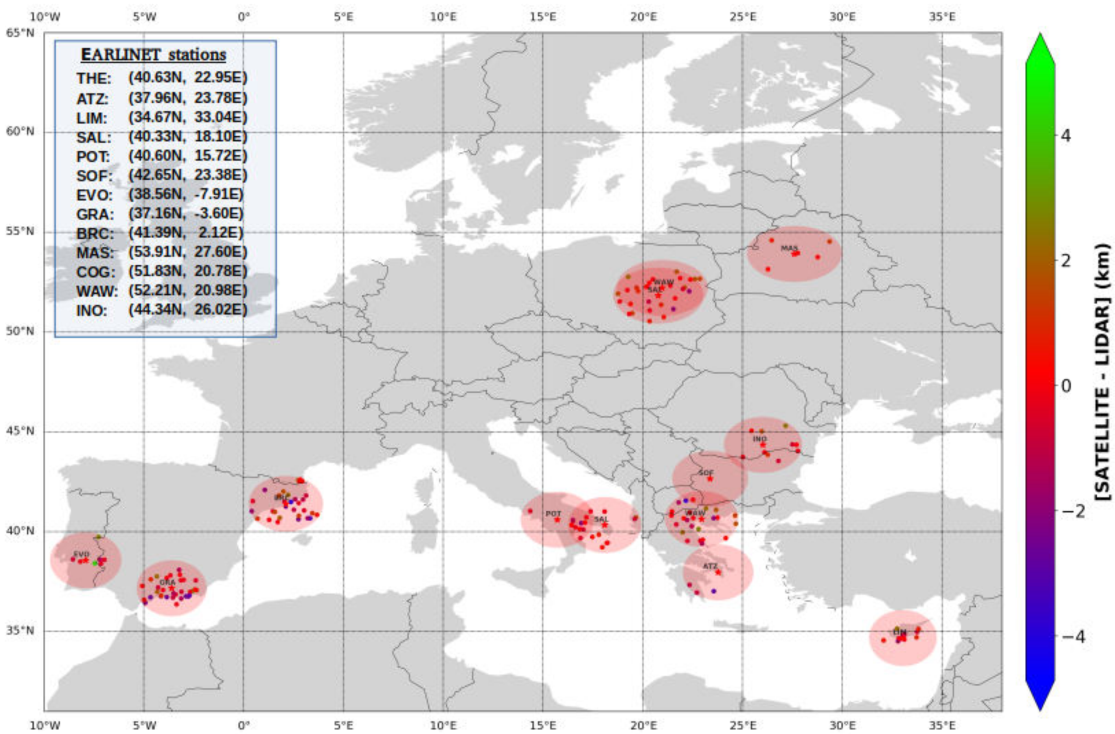

Figure 5. Spatial distribution of collocated layers. The concentric red circles denote regions of 150 km from the location of EARLINET stations Refer to Table 4 for the EARLINET code names shown in the legend.

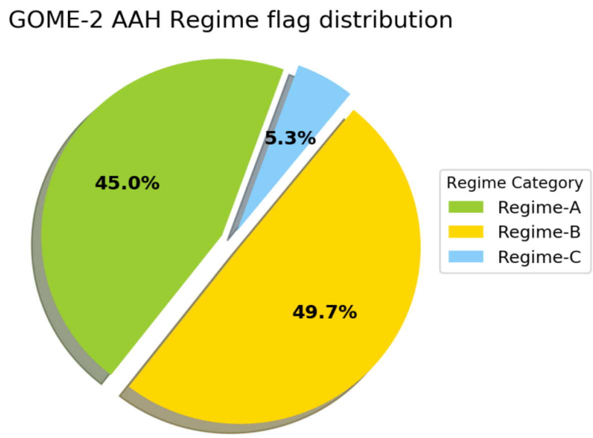

Figure 6. Distribution of reliability category (Regime flag) of the selected collocated observations as per Sect. 3.1.2.

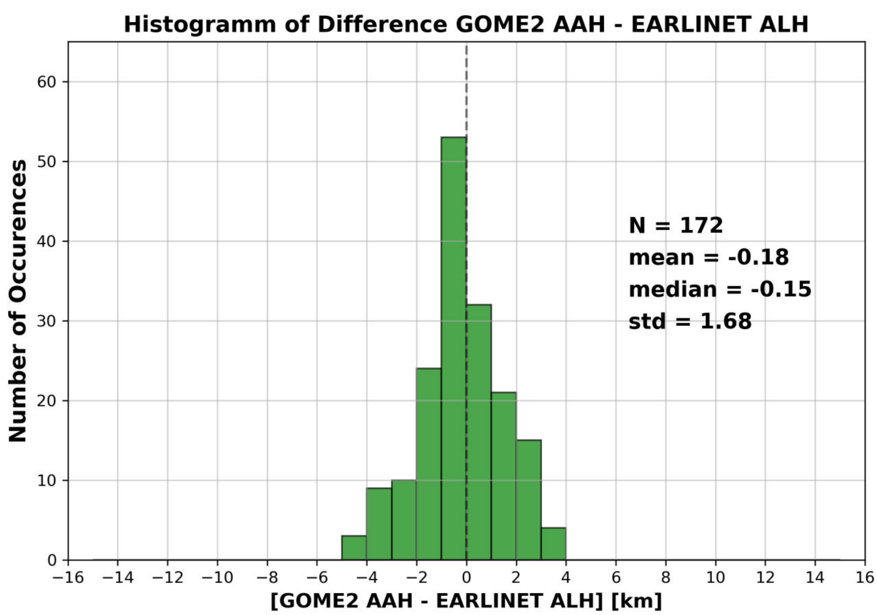

Figure 7. Histogram of absolute differences between GOME-2 Absorbing aerosol height and aerosol layer height obtained from EARLINET backscatter profiles (using the WCT method), calculated for all collocated cases.

https://doi.org/10.5194/acp-2020-601
Preprint. Discussion started: 8 July 2020

Atmospheric Chemistry and Physics
Open Access
EGU
Discussions

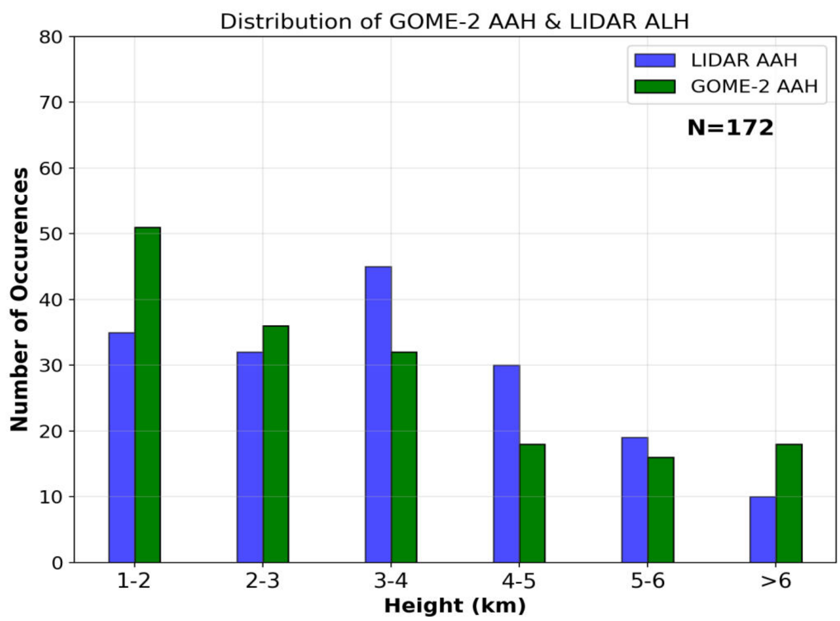

Figure 8. Bar plot of GOME-2 AAH (green) and EARLINET ALH (blue) stations occurrences. The height ranges of bins are between 1-2, 2-3, 3-4, 4-5, 5-6 and > 6 km.

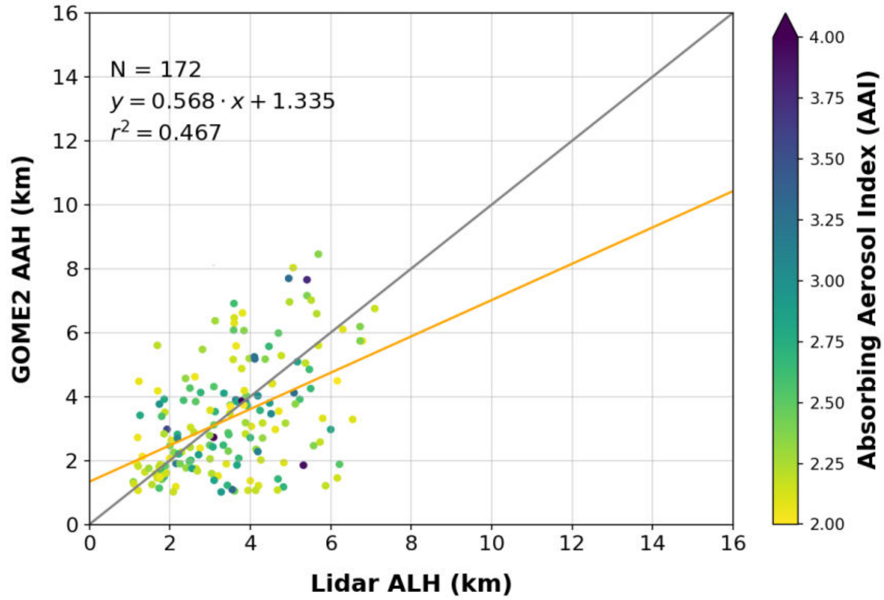

Figure 9. Scatterplot between GOME-2 AAH and aerosol layer height from EARLINET stations, for the total of collocated cases. The associated AAI value is colour coded.

https://doi.org/10.5194/acp-2020-601
Preprint. Discussion started: 8 July 2020

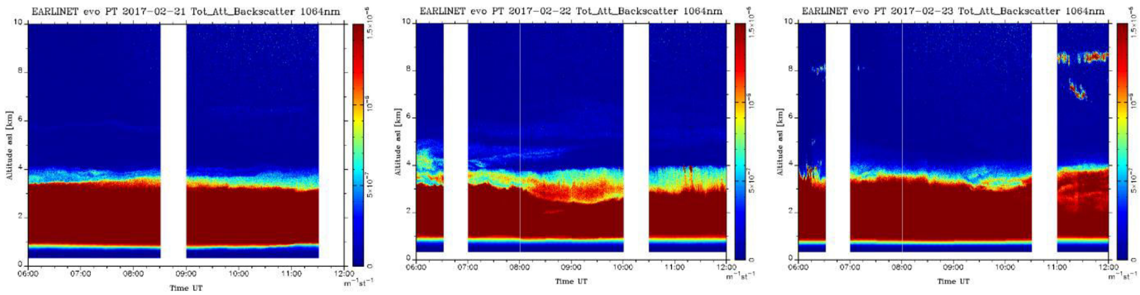

Figure 10. Quicklook images corresponding to the total attenuated backscatter at 1064 nm observed with the EARLINET Évora lidar for the 21st (left), the 22nd (middle) and the 23rd (right) of February 2017 show nicely the evolution of this particular dust event (https://quicklooks.earlinet.org/) (Blue colors indicate weak backscattering signal and yellow and red colors indicate higher backscattering signal)

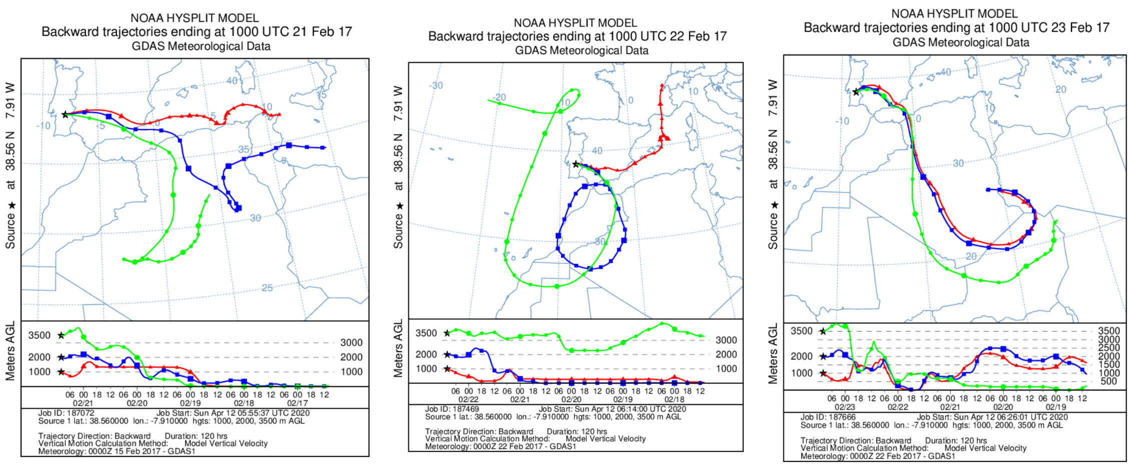

Figure 11. The 5-day NOAA HYSPLIT backward trajectories ending at the position of Évora 10:00 UTC (38.56°N, -7.91°E) for the 21st (left), the 22nd (middle) and the 23rd (right) of February show nicely the evolution of this particular dust event.

https://doi.org/10.5194/acp-2020-601
Preprint. Discussion started: 8 July 2020

Atmospheric Chemistry and Physics
Discussions

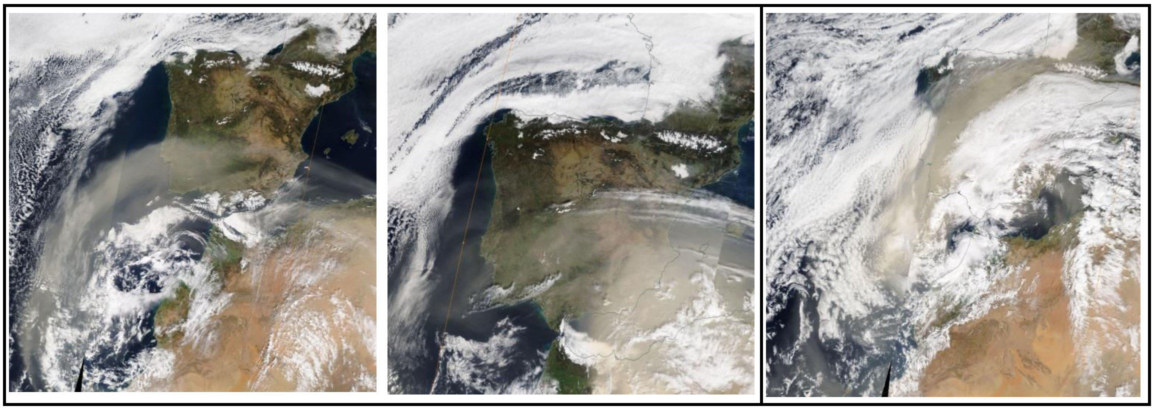

Figure 12. Images of Saharan dust transport as captured by the MODIS/Terra satellite, on the 21st (left), the 22nd (middle) and the 23rd (right) of February 2017, over the Iberian Peninsula. The orange line denotes the Terra overpasses on the 21st (~11:00), 22nd (~12:00) and 23rd (~11:00) of February 2017 (https://worldview.earthdata.nasa.gov/).

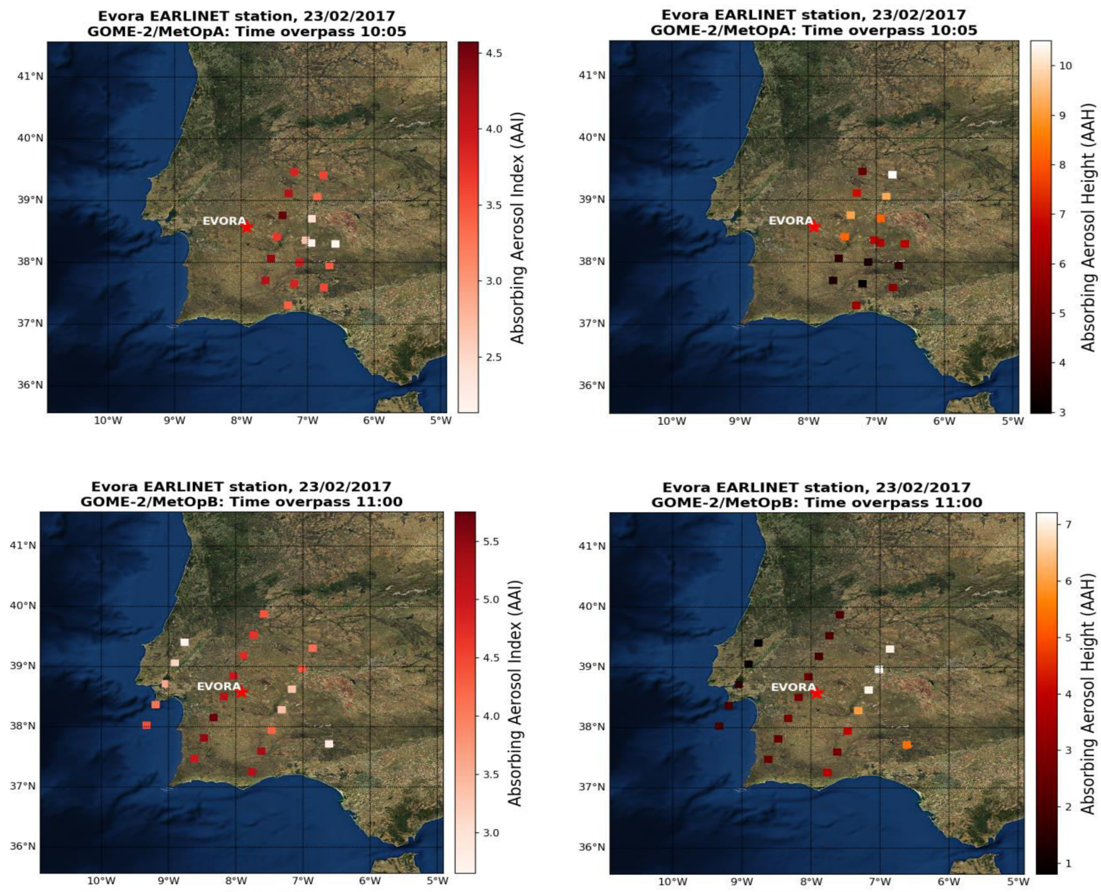

Figure 13. The Saharan dust transport on the 23rd of February 2017 over the Iberian peninsula. The Evora station is marked with the red star. The color schemes illustrate the altitude of the AAH (right) and the AAI (left) as observed by GOME-2A (upper panel) at 10:00 UTC and GOME-2B (bottom panel) at 11:00 UTC.

https://doi.org/10.5194/acp-2020-601
Preprint. Discussion started: 8 July 2020

Atmospheric Chemistry and Physics
Discussions

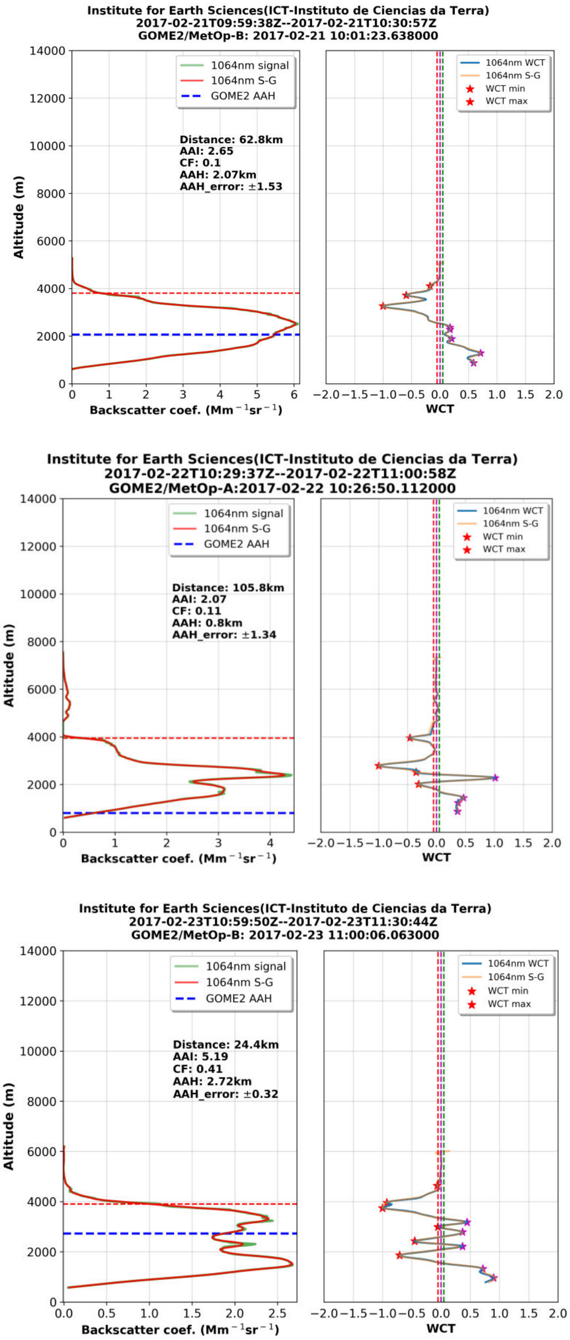

Figure 14. Evora lidar backscatter profiles (red and green lines, left subpanels) and WCT method applied at 1064nm (stars, right subpanels) and GOME-2A, GOME-2B AAH (blue dashed line) and associated error, AAI, CF and distance (legend) for the 21st (top), the 22nd (middle) and the 23rd (bottom) of February.

https://doi.org/10.5194/acp-2020-601
Preprint. Discussion started: 8 July 2020

Atmospheric Chemistry and Physics
Discussions

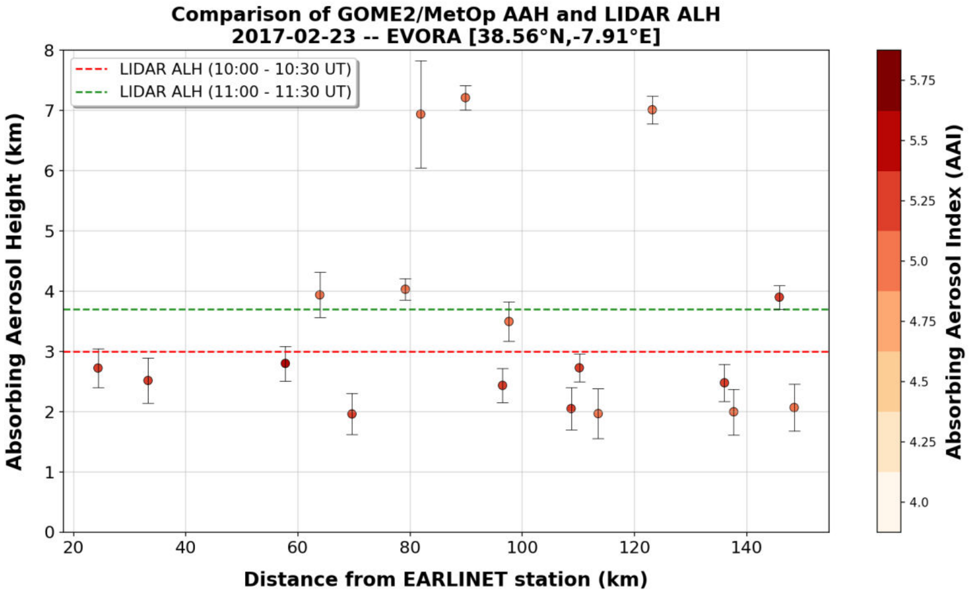

Figure 15. GOME-2 AAH (coloured dots) against the distance of the retrieved pixels from EVORA lidar station, on the 23rd February, 2017. The color scale on the right indicates the Absorbing Aerosol Index (AAI) for GOME-2 pixels. The two dashed lines correspond to the simultaneous lidar observations at 10:00-10:30 UT (red) and 11:00-11:30 (green)